Cambridge Centre for Computational Chemical Engineering

University of Cambridge

Department of Chemical Engineering

Preprint ISSN 1473 – 4273

A simple model for the aggregate structure of soot particles

Robert Patterson, Neal Morgan,

Markus Kraft [1]

released: 13 September 2006

[1] Department of Chemical Engineering
University of Cambridge
Pembroke Street
Cambridge CB2 3RA
UK
E-mail: mk306@cam.ac.uk

Preprint No. 38

c4e

Key words and phrases: modelling, aggregation, coagulation, soot, fractal

Edited by
Cambridge Centre for Computational Chemical Engineering
Department of Chemical Engineering
University of Cambridge
Cambridge CB2 3RA
United Kingdom.

Fax: + 44 (0)1223 334796
E-Mail: c4e@cheng.cam.ac.uk
World Wide Web: http://www.cheng.cam.ac.uk/c4e/

Abstract

New bivariate models, without free parameters, for soot particle structure are introduced to qualitatively replicate observed particle shapes and are found to offer quantitative improvements over older single variable models. Models for the development of particle shape during surface growth and for particle collision diameters are set out, and implemented along with two models taken from other published work. Using a stochastic approach, bivariate soot particle distributions are calculated for the first time. Distributions calculated for the new models are found to be insensitive to the collision diameter model used for coagulation. The total mass of soot produced in a laminar premixed flame is found to vary by no more than 20% as the model for the geometric effects of chemical reactions on the surface of particles is changed. Histories of individual particles are analysed and show the limitations of collector particle techniques.

Contents

1 Background

The fractal nature of large soot particles has been known for some time from electron micrographs, for examples from diffusion flames see [32, 15] and an example from a premixed flame is given in [39]. The extensive review paper [30] gives an indication of how much work has been done on experimental techniques to measure the properties of these fractal structures. Detailed consideration of how to account for the assumed fractal nature of soot particles from road vehicles has even been included in atmospheric modelling [10].

Simulation or prediction of the fractal structure of soot particles is at a less advanced stage. Mitchell and Frenklach started to investigate soot aggregation in [17, 18, 19] by representing a single 'collector' particle as a union of intersecting spheres. The natural extension of this work to a population of particles with structures represented as a union of spheres is presented in [5], but this is very computationally expensive. A huge simplification of the model, including an assumption that particle size and structure are independent, and incorporating a numerical fit for the functional form of the particle collision diameter, enables very fast calculations to be made for the lower moments of the particle mass distribution and a measure of mean shape [3]. These 'method of moments' calculations seem to offer considerable insight into the development of particle structure, although it is difficult to assess the significance of the different modelling approximations using their numerical framework—the method of moments with interpolative closure [8].

Park and Rogak [23] added a partial representation of aerosol particle structure to a one dimensional sectional technique and produced software designed to simulate a plug flow reactor [24]. Their work differed from the approach of Frenklach and his co-workers by representing particle structure with a quantity which has a simple physical meaning—the average number of primary particles per aggregate, with a separate average being taken within each size section. To calculate particle collision diameters from this information an assumed fractal dimension of 1.8 was used [37, 38] which implies a very open particle structure. This value of 1.8 has been used by other authors, for example, in [33] and reported from diffusion flame soot TEM images in [14]. Slightly lower values were obtained from light scattering experiments on premixed methane-oxygen flames in [31].

In [13] the influence of fractal dimension on coagulation rates is discussed and reported to be small in the continuum regime (particles large compared to the free path) but to be significant in the free molecular regime (particles small compared to the free path). Since smaller soot particles will be in the free molecular regime even at elevated pressures (for example, a 5 nm particle at 10 bar) exploration of models for the collision cross-section such as assumed fractal dimensions seems desirable. The importance of this is emphasized by the TEM images in [21] which show soot particles from a laminar premixed ethylene flame which are not really fractal and, despite the results mentioned in the previous paragraph, do not seem to have a fractal dimension as low as 1.8.

The purpose of the work reported in this paper is to introduce and test simple models for the aggregate structure of soot particles with the first fully bivariate simulations of soot formation. Understanding the properties of these models is a critical first step in building simulations with realistic models for soot surface chemistry. Without such simulations

it will be impossible to progress from the descriptive fits of [40, 12, 1] to mechanistic models. Simulation of particle structure will also enable more careful comparisons with experimental data based on particle mobility sizing [41, 16] and scattering techniques such as those discussed above and, for example, [36] and [6].

2 Framework

2.1 The flame

To keep the physical system as well defined as possible this work concentrates exclusively on laminar premixed flames. The soot model, an extension to which is described below, is introduced in [1] on the assumption of spherical particles and based on the gas phase chemistry from [35]. In this model soot particles are assumed to form exclusively through the coalescence of two pyrene molecules to make a (spherical) particle of 32 C atoms. Particle growth is possible by surface deposition of further pyrene molecules and addition reactions involving acetylene. Surface oxidation by oxygen (O_2) and hydroxide ions (OH) is included. For all the flames looked at it was found that addition of acetylene to the surface of soot particles was the main route by which mass moved from the gaseous to the solid phase.

2.2 Numerical method

All simulations reported in this paper used the Linear Process Deferment Algorithm [25], an acceleration of the established Direct Simulation Algorithm (DSA) [2, 7]. Details of the soot model in the context of DSA computation under the assumption of spherical particles are given in [2, 26].

2.3 Particle shape variable

Soot modelling has generally concentrated on particle mass or volume and used a constant density assumption. Therefore mass or volume has been used as the independent variable for describing each soot particle. The equivalence of mass and volume follows from the assumption that all soot material has the same density and the work reported here uses the value supplied with the soot mechanism [1] as implemented by its authors [28]: 1.8 g cm^{-3}.

In this paper mass and surface area are used as the independent variables in the particle descriptions or types, which are thus pairs of positive real numbers. Surface area is used rather than the number of primary particles as in [23] because it gives a description immediately equivalent to that of the shape descriptor in the Mitchell and Frenklach work [17, 18, 19].

2.4 Notation

For convenience the following dimensionless functions of a particle type are defined, the quantities are divided by their value for newly incepted particles (type x_0) so they all take the value 1 at x_0. (x_0 describes a spherical particle of 32 C atoms—the assumed form of all newly incepted particles.)

- $c(x)$ the collision diameter of the particle
- $m(x)$ the mass of the particle
- $s(x)$ the surface area of the particle
- $v(x)$ the volume of the particle ($= m(x)$ due to the constant density assumption)

A shape descriptor d is defined in [18, 3] by

$$d(x) = \frac{\log(s(x))}{\log(v(x))} \tag{1}$$

and hence setting $d(x_0) = \frac{2}{3}$ (the value would otherwise be undefined at x_0) yields $\frac{2}{3} \leq d \leq 1$. Note that for a sphere, given x_0, any two of d, v and s define the value of the third, and that d depends on x_0 via the normalisation of v and s.

3 Models for lengths

3.1 Collision diameter

The collision cross-section or diameter of particles describe how much space they sweep out as they move around. As mentioned in the introduction, the coagulation rate is much more sensitive to collision diameter models in the free molecular regime than in the continuum regime. This is not especially surprising given the form of the coagulation kernel between two particles [13] in the continuum regime:

$$K^{cn}(x,y) \propto (c(x)+c(y))\left(\frac{1}{c(x)}+\frac{1}{c(y)}\right) = 2+\frac{c(x)}{c(y)}+\frac{c(y)}{c(x)}. \tag{2}$$

This only depends on the ratio of collision diameters of the two particles not their absolute value and so some kind of cancellation may be expected if both are increased. However, the free molecular kernel [13]:

$$K^{fm}(x,y) \propto \left(\frac{1}{m(x)}+\frac{1}{m(y)}\right)^{\frac{1}{2}} (c(x)+c(y))^2 \tag{3}$$

scales with the square of the absolute value of the collision diameters.

In the spherical particle model the collision diameter of the particles are simply taken to be the ordinary diameters of the spheres, and so with the scaling of §2.4 $c(x) = v(x)^{\frac{1}{3}}$. In this section ways to proceed for non-spherical particles are set out.

3.1.1 Mitchell & Frenklach collision diameter

In detailed work by Mitchell and Frenklach, in which aggregates were represented as collections of intersecting spheres [18, 17], the collision cross-section was expressed in terms of the radius of gyration. The radius of gyration was calculated using a time consuming Monte Carlo integration which is distinct from the Monte Carlo simulation method. Mitchell's thesis [18] also proposed the following model as a practical approximation for use in further work:

$$\begin{aligned} c_{agg}\left(x\right) &= kv(x)^{\frac{1}{3}} + 2\left(1-k\right)\left[\frac{\left(av(x)^{\frac{1}{3}}\right)^{b} + v(x)^{b}}{\left(a2^{\frac{1}{3}}\right)^{b} + 2^{b}}\right]^{\frac{1}{b}} \\ a &= \quad 1.53311 \\ b &= -1.35419 \\ k &= \quad 0.43074. \end{aligned} \tag{4}$$

This was extended to general particles by interpolation using the shape descriptor d to give

$$c(x) = 3\left[\left(d\left(x\right) - \frac{2}{3}\right)c_{agg}\left(x\right) + \left(1 - d\left(x\right)\right)v(x)^{\frac{1}{3}}\right]. \tag{5}$$

3.1.2 Balthasar & Frenklach collision diameter

Balthasar and Frenklach [3] went even further in simplifying the work mentioned in §3.1.1. They introduced a correlation derived from the more detailed work which expressed collision cross-section as a function of aggregate volume and shape descriptor (equivalently surface area):

$$c(x) = \left(2.7375 \times d\left(x\right) - 0.825\right) \times v(x)^{\frac{1}{3}}. \tag{6}$$

By making some further approximations, in particular that at any time the shape descriptor was the same for all particles, they were able to use the method of moments with interpolative closure (MoMIC)[8] and so achieve very short computational times.

3.1.3 Arithmetic mean collision diameter

To test the sensitivity of results to the exact collision cross-section model the arithmetic mean of the volume and surface equivalent diameters was used:

$$c(x) = \frac{1}{2}\left(v(x)^{\frac{1}{3}} + s(x)^{\frac{1}{2}}\right). \tag{7}$$

This barely deserves to be called a model but it seems to be about the simplest expression that uses the information contained in the surface area and the volume.

3.1.4 Weighted geometric average collision diameters

A second alternative considered was the geometric mean of the equivalent volume and surface diameters

$$c(x) = v(x)^{\frac{1}{6}}\, s(x)^{\frac{1}{4}}\,. \tag{8}$$

This is a member of the family of weighted geometric averages

$$c(x) = v(x)^{a}\, s(x)^{b} \tag{9}$$

which satisfy

$$3a + 2b = 1. \tag{10}$$

These turn out to have an interesting connection to assumed fractal dimensions: Consider an idealised aggregate soot particle of volume V, surface area S consisting of n_p spherical primary particles of diameter d_p in point contact with each other (the model used in [22]). Solving for n_p and d_p gives

$$d_p = \frac{6V}{S} \tag{11}$$

$$n_p = \frac{S^3}{36\pi V^2} \tag{12}$$

The standard fractal relationship, in this case for collision diameter C and aggregate volume is

$$n_p = k\left(\frac{C}{d_p}\right)^{D} \tag{13}$$

where k is the fractal prefactor and D the fractal dimension. Assuming $k = 1$, which is necessary to make the formula consistent for a sphere (note that most published data is for twice the radius of gyration rather than the collision diameter as used here, so different values of k are reported) one finds [33, equation 4]

$$C = 6 \times (36\pi)^{-\frac{1}{D}}\; V^{1-\frac{2}{D}}\; S^{\frac{3}{D}-1}. \tag{14}$$

For a general particle x this becomes, in the dimensionless quantities of §2.4,

$$c(x) = v(x)^{1-\frac{2}{D}}\, s(x)^{\frac{3}{D}-1} \tag{15}$$

which is in the form of (9) and satisfies (10).

One sees that using the equally weighted geometric mean collision diameter (8) is essentially the same as assuming a fractal dimension of 2.4 and that a fractal dimension of 1.8 implies $a = -\frac{1}{9}$ and $b = \frac{2}{3}$. The negative value of a is a somewhat counter-intuitive but cannot easily be dismissed because of the extensive reports of soot particles with a fractal dimension of 1.8, some of which were referred to in the introduction above.

3.2 Radius of curvature

Electron micrographs show soot particles are quite smooth over lengths considerably greater than the size of newly incepted soot particles. Therefore aggregates composed of small soot particles must be smoothed after they coagulate. For a discussion of this issue see [4] and the references cited therein. The authors of [4] conclude that this smoothing is largely the result of chemical deposition on the surface of soot aggregates.

In the context of the two variable model for soot particles used in this paper such surface reactions (and any that remove mass) must be defined by the changes they cause in particle mass and surface area. The particle mass change is obvious—it is the mass of the deposited molecule—and the volume change is simply this value divided by the density. For a sphere (initial radius R, surface area S viewed as functions of volume V) the change in surface area is also trivial; the differential form is

$$\frac{\mathrm{d}}{\mathrm{d}V}S = \frac{2}{R}. \tag{16}$$

The relationship between the volume and surface increments in controlled by the tightness of the surface curvature, so for any shape other than a sphere it depends on position. For a general shape the value of R which makes (16) true at a point is known as the radius of curvature at that point (strictly there are two radii of curvature at each point on a three-dimensional surface and an average is needed, but that extra complexity is redundant here). As one might expect the radius of curvature at a point is the radius of a circle which best fits a small line segment on the surface at that point.

The correct expression for the radius of curvature of non-spherical particles in the bivariate model considered here is not at all obvious. Physical considerations, principally TEM data, for example, [32, 15, 21], suggest that any radius of curvature should at least cause particles to become rounder. To make the idea of rounding more precise the following criteria were used:

1. spherical particles must remain spherical in the limit of small volume increments;
2. all particles must be geometrically possible, in particular the surface to volume ratio must be achievable;
3. non-spherical particles must become rounder during surface growth;
4. non-spherical particles must become rounder during surface oxidation.

Note that 3 & 4 are not the only possibilities, in particular, provided particles never become less round as a result of surface reactions, it is not necessary that every instance of every surface reaction cause a strictly positive increase in roundness.

One consequence of these conditions is that at least two radii of curvature (these are not the principal radii of curvature from differential geometry) are required for non-spherical particles, one to use when $\Delta V > 0$ and the other when $\Delta V < 0$. The following lengths were used in this work:

$$R_{gr} = \left(\frac{S_{old}}{4\pi}\right)^{\frac{1}{2}} \tag{17}$$

for growth processes and

$$R_{ox} = \frac{3V_{old}}{S_{old}} \tag{18}$$

for oxidation processes.

In the scaled, dimensionless style of §2.4 we have, using (16)

$$r_{gr}(x) = s(x)^{\frac{1}{2}} \tag{19}$$

and

$$r_{ox}(x) = \frac{v(x)}{s(x)}. \tag{20}$$

So for $\Delta v > 0$

$$\Delta s = \frac{2}{3}\,\Delta v\; s(x_{init})^{-\frac{1}{2}} \tag{21}$$

and for $\Delta v < 0$

$$\Delta s = \frac{2}{3}\,\Delta v\,\frac{s(x_{init})}{v(x_{init})} \tag{22}$$

where x_{init} is the initial state of the particle.

Other definitions are possible and numerical tests of the simpler, possibly less realistic, case $r_{gr}(x) = r_{ox}(x) = c(x)$ are reported below. The factor of $\frac{1}{2}$ that might be expected in this last equation is absorbed in the scaling defined in §2.4.

4 Model Comparison

4.1 Bulk Properties

To investigate the significance of the modelling assumptions, bulk properties of the particle populations predicted using the different models were compared for the 10 bar laminar premixed ethylene flame JW10.673 [11], which was also the focus of [3]. Results are shown in figures 1–4 and a summary of the different models along with the names used in the legends of the figures is given in table 1. Further information on the flame and simulation results can be found at [9].

The simulation method followed [2]: The flame chemistry was first calculated using a MoMIC [8] approximation to account for the effects of soot. The chemical species profiles produced in this way were then provided as input to the stochastic soot code.

Monte Carlo methods introduce some random noise into the results and in figures 1–4 the values shown are averaged over 20 realisations of the Markov processes. The estimated 95% confidence intervals for the volume fraction, second mass moment and surface area density are less than $\pm 2\%$ of the plotted average values.

The results shown in figures 1–4 indicate that the differences between the different models for particle shape are generally smaller than the difference between the spherical particle model and the closest non-spherical model. The differences between the values calculated

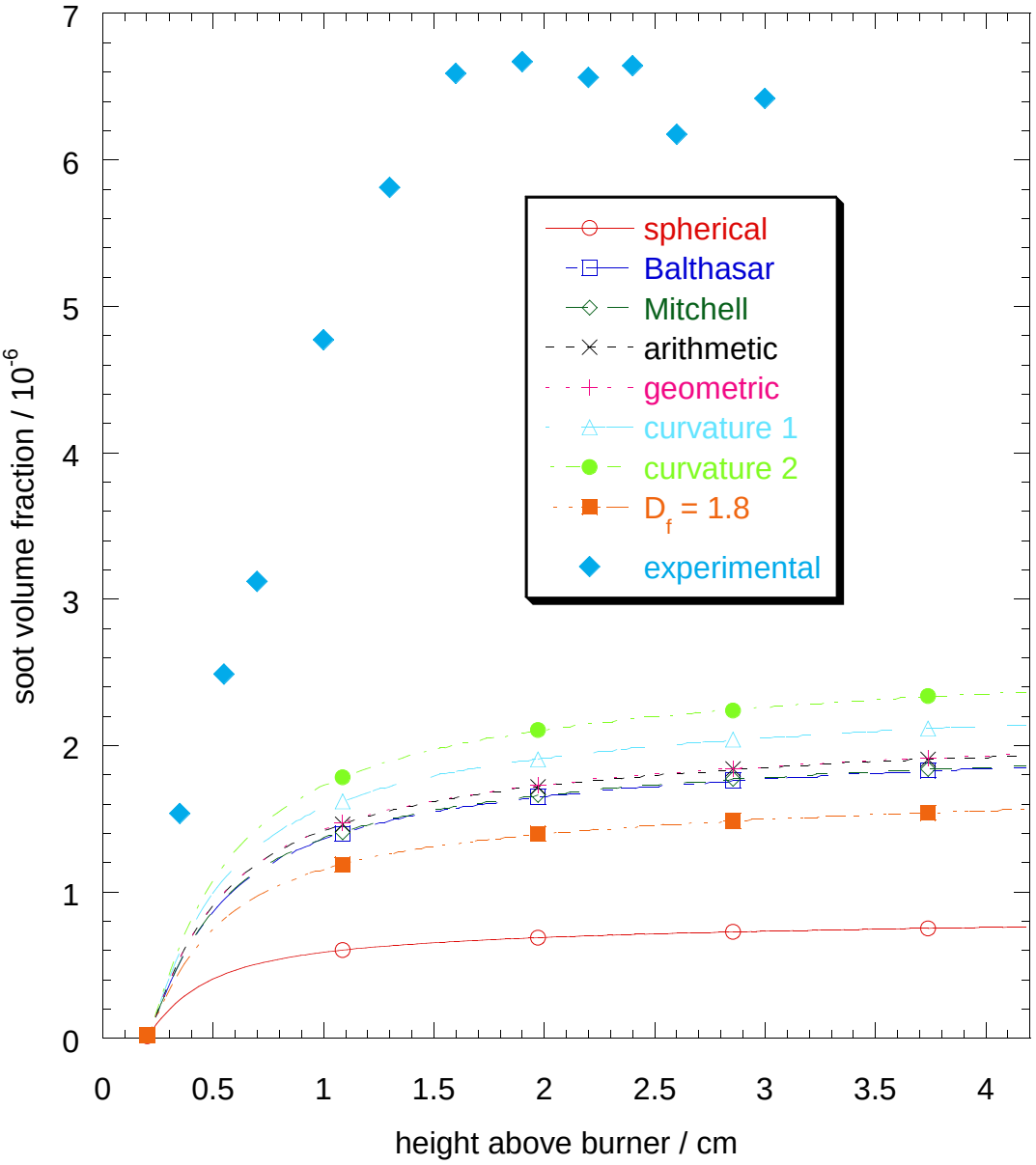

Figure 1: *soot volume fraction*

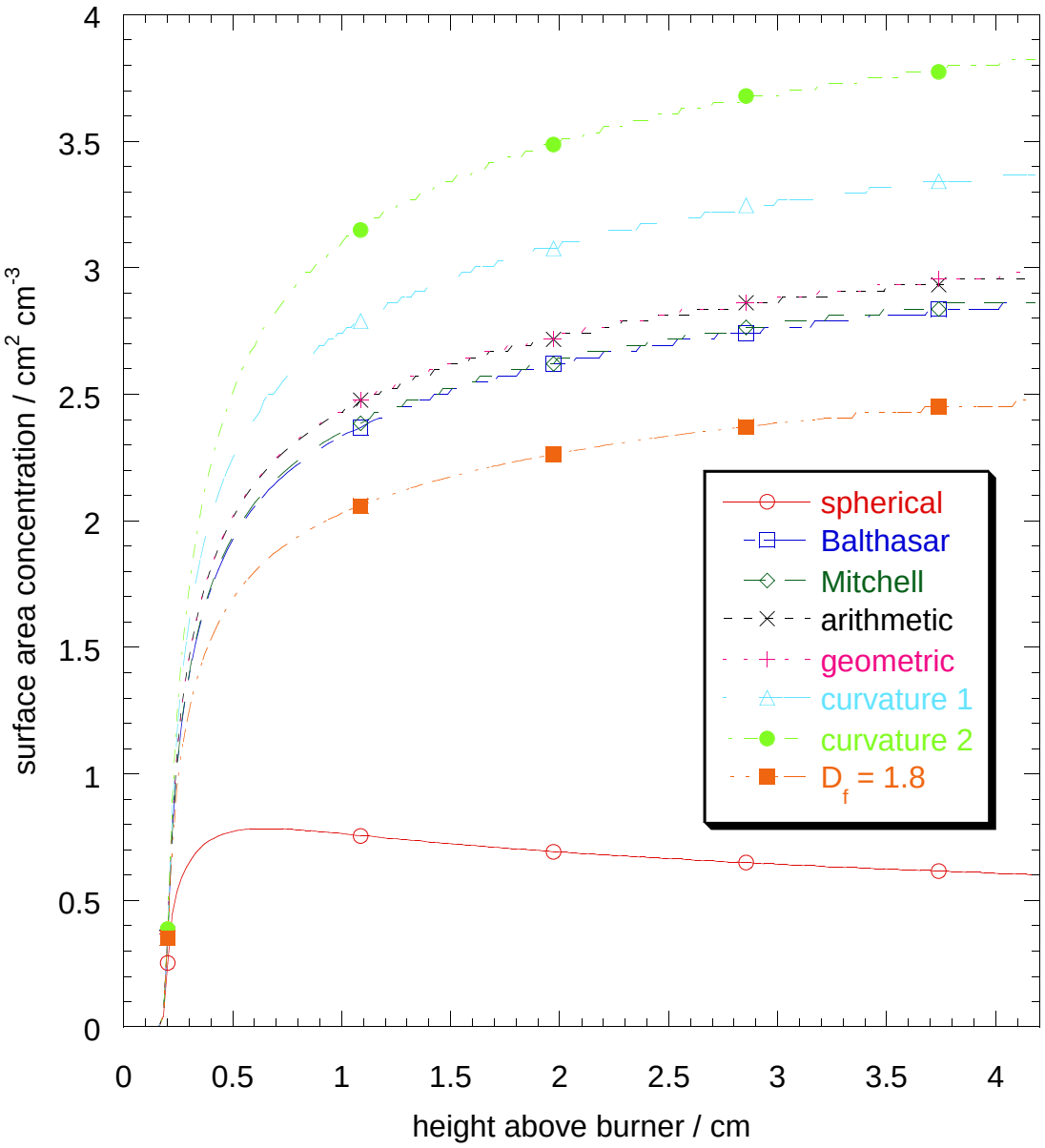

Figure 2: *surface area per unit volume*

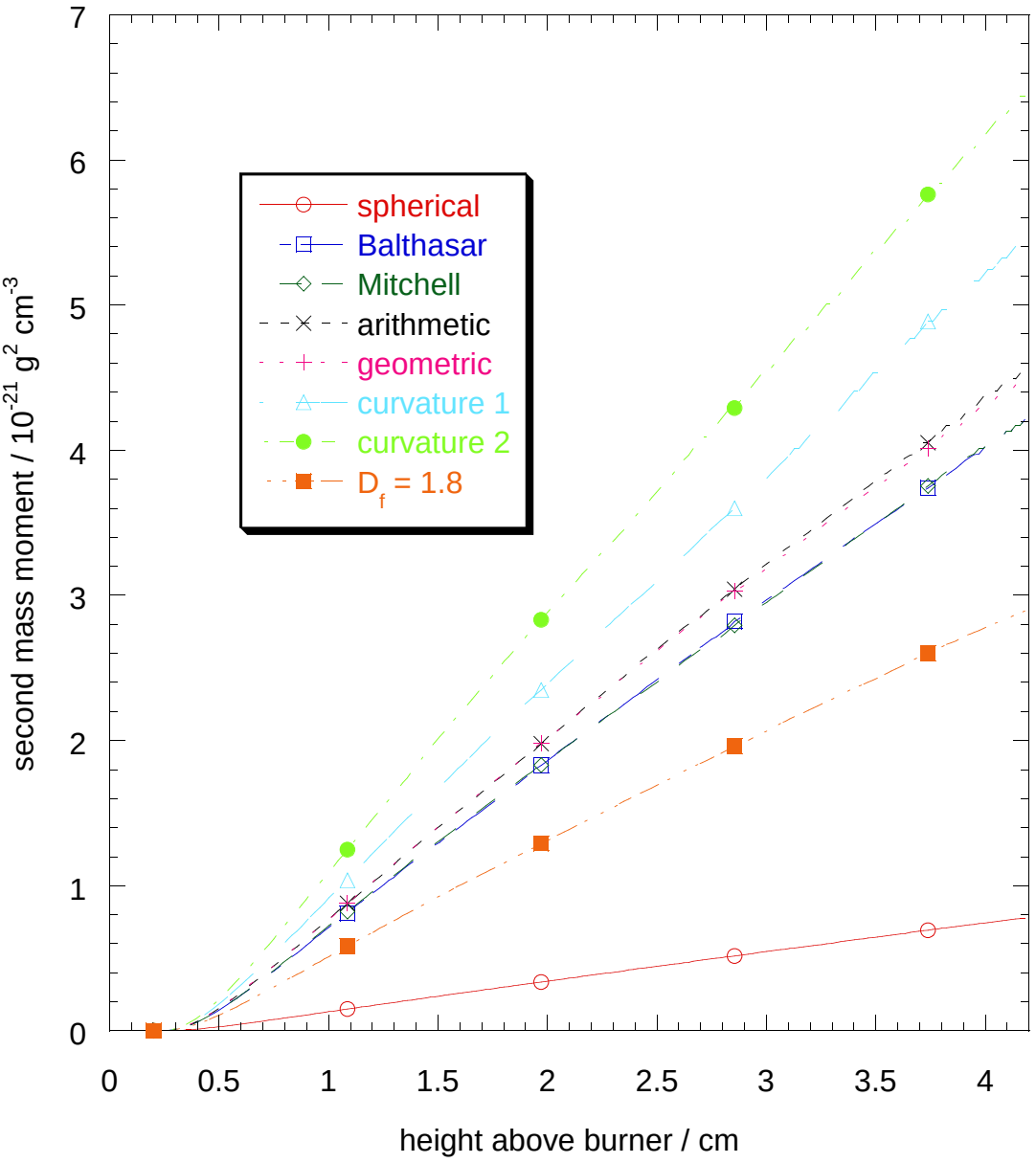

Figure 3: *second mass moment*

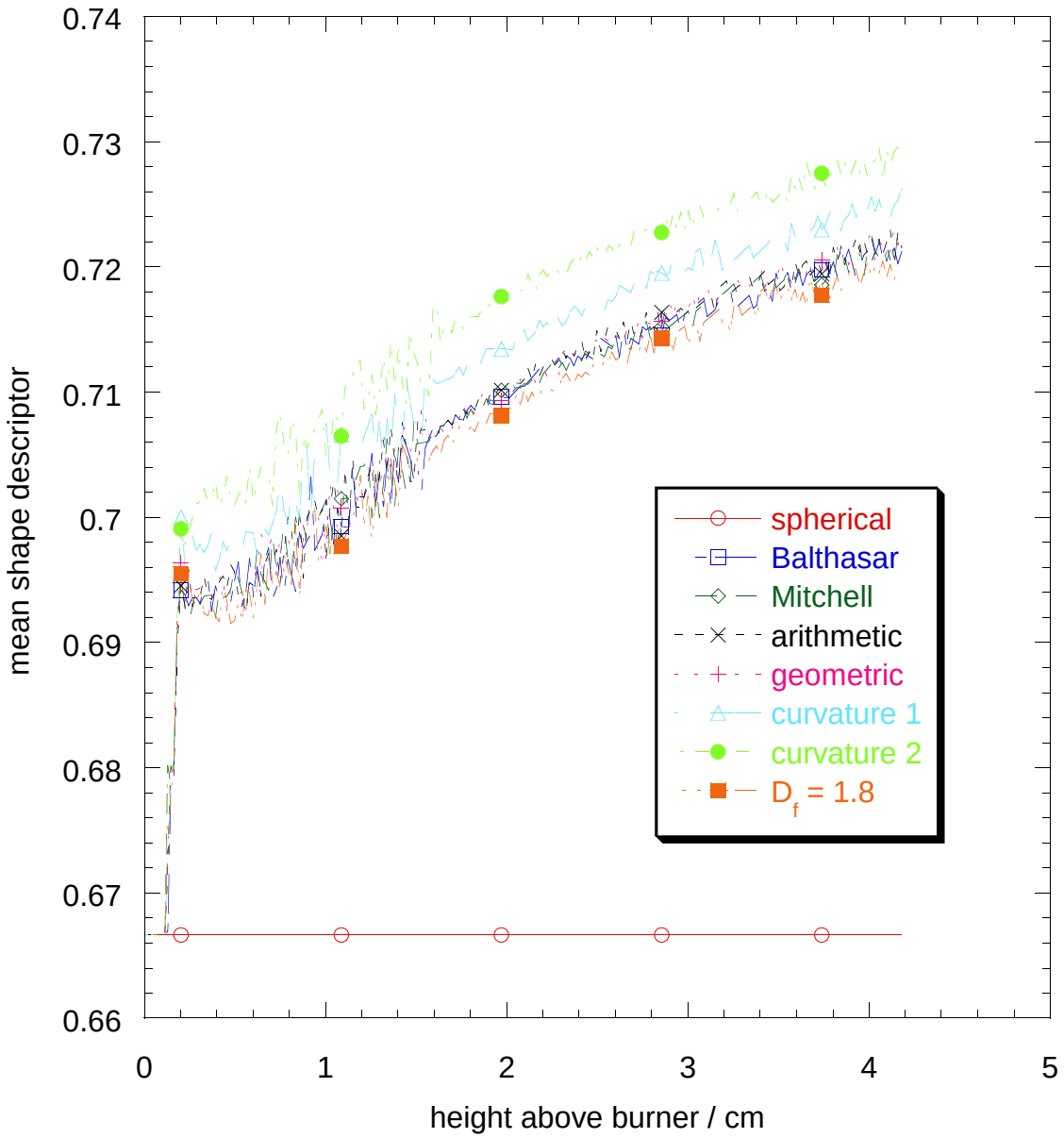

Figure 4: *mean shape descriptor*

using the collision diameters of Balthasar (& Frenklach)(6), Mitchell (& Frenklach) (5), the arithmetic mean (7) and the geometric mean (8) are particularly small. If these were the only models available one would conclude that the exact choice of collision diameter model was not significant provided one did not assume particles were spherical. In [25] it was noted that C_2H_2 addition was the dominant process in soot growth in two flames similar to the one studied here. According to the soot chemistry model [1, 35]the rate of C_2H_2 addition is proportional to particle surface area which is why all the non-spherical models predict larger soot volume fractions than the spherical particle model.

However, the results with collision diameter calculated assuming all the primary particles in an aggregate are the same size and that all aggregates have a fractal dimension of 1.8 (see §3.1.4) show a significant deviation from all the other collision diameter models. Significant differences are also seen for the alternative radii of curvature models and these will be discussed below. The assumed fractal dimension model does not have a noticeable effect on number density compared to the other models (results for number density are not plotted but, after the initial spike, they differ from the results for the geometric mean collision diameter model by less than 5%), however, it leads to a significant reduction in surface area and in the soot volume fraction. The reduction in soot volume fraction predicted by the $D_f = 1.8$ model compared to the other non-spherical models appears to be due to enhanced OH oxidation rates. The soot chemistry model treats OH oxidation as a collision controlled process with rate proportional to the square of the collision diameter of particles. Particle collision diameters are generally much larger under the $D_f = 1.8$ model than under the other models so the OH oxidation rate is also higher. This explanation was verified by performing simulations with the $D_f = 1.8$ model but with the OH oxidation rate calculated with the equivalent volume sphere diameter in place of the particle collision diameter. The soot volume fraction calculated by the modified simulation was within 1% of that calculated using the geometric mean collision diameter. This illustrates how important good models of particle shape are in order to correctly predict reactions between particles and the surrounding gas phase.

As mentioned is §3.2 it is necessary to investigate the importance of the models for particle curvature. This was done using the models named 'curvature 1' and 'curvature 2' as specified in table 1. From the results shown in figures 1–4 one sees that as the radii of curvature used are brought closer to the collision diameter (thus making particles less smooth) the consequent increase in particle surface area leads to additional surface growth and thus a higher soot volume fraction. The difference in simulated soot volume fraction between 'curvature 2' and the geometric mean collision diameter model from which it is derived is much smaller than the difference between both of these models and the spherical particle model. This means that while uncertainty about surface curvature is a concern it does not prevent further work.

4.2 Particle Size Distributions

The particle distributions simulated with the geometric mean collision diameter model (see table 1) at 0.4 cm and 4.2 cm above the burner face are shown in figure 5. The distributions are shown in two ways—as a scatter plot in surface-volume space and as a density on the volume axis. The smooth densities were calculated from the discrete

data using a Gaussian blurring technique; specifically, with the 'density' function of the computer statistics package R [27]. More details can be found in the online documentation and in [34, §5.6]. The distributions for the other models are qualitatively the same but with quantitative differences at large particle sizes.

The most important feature of figure 5 is that, in both cases, the distribution is concentrated on a line. At 0.4 cm above the burner the line is noticeably curved for volumes less than 10^{-17} cm^3 but otherwise the lines are straight. Since the distributions appear concentrated on these straight lines, it is natural to perform a linear regression to find the slope. From these slopes (the intercept terms were negligible) one can infer a primary particle diameter by assuming all soot particles are composed of primary particles of the same size and in point contact. Diameters calculated in this way are given in table 2.

For each height above the burner the primary particle diameters given in table 2 are quite similar (within 5% of the value for the Balthasar model), even for the curvature 2 model which leads to a noticeably different soot volume fraction (see figure 1). The closeness of the values would making testing the models by comparing primary particle diameters to those observed by electron microscopy very difficult. This supports the view that any reasonable approximation for the aggregate structure of soot particles is sufficient given the current relative imprecision of the chemical mechanisms involved in soot formation and growth.

4.3 Individual particle behaviour

To get an understanding of why different models might lead to similar results particles a small volume of gas moving through the laminar premixed ethylene flame JW10.673 ([11]) used previously were observed. In the upper half of figure 6 the time evolution of the shape descriptor (1) is plotted for two of these particles. The bottom left panel, figure 6(c), tracks the size of the same two particles in the simulation, which used the Balthasar and Frenklach collision diameter model (6). The top right panel, figure 6(b), gives a more detailed view of the very active early life of the particles until just after the point at which they coagulate with each other (this point is circled on the plot). On this more detailed plot one sees abrupt upward jumps in the ratio when the particle undergoes coagulation followed by periods of smooth decrease as surface growth makes the particle more round according to §3.2. The bottom right panel, figure 6(d), is included to show that two particles chosen from a simulation using the 'curvature 2' model (see § 3.2) do not behave very differently to the two from the Balthasar model simulation.

All four plots show an early period of rapid activity in which the shape descriptor undergoes damped oscillations and size grows steadily. The final shape and size of the particles however, are largely determined by a few coagulation events after the initial activity has subsided. Figure 6(c) gives a very clear view of how chemical reactions with the surface of the soot particles all occur relatively close to the burner face as shown by the smooth growth in particle size. Figure 6(b) illustrates the way that these surface reactions largely negate the shape changing effects of the coagulation that occurs up to 0.5 cm. Because of this cancelling out, a detailed model of the rapid processes may not be necessary for many purposes. For flames similar to JW10.673 it my be sufficient to predict the outcome

Table 1: *Simulated length models for JW10.673*

name	$c(x) =$	$r_{gr}(x) =$	$r_{ox}(x) =$
spherical	$v(x)^{\frac{1}{3}}$	$v(x)^{\frac{1}{3}}$	$v(x)^{\frac{1}{3}}$
Balthasar	$(2.7375 \times d(x) - 0.825) \times v(x)^{\frac{1}{3}}$	$s(x)^{\frac{1}{2}}$	$\frac{v(x)}{s(x)}$
Mitchell	see [18]	$s(x)^{\frac{1}{2}}$	$\frac{v(x)}{s(x)}$
arithmetic	$\frac{1}{2}\left(v(x)^{\frac{1}{3}} + s(x)^{\frac{1}{2}}\right)$	$s(x)^{\frac{1}{2}}$	$\frac{v(x)}{s(x)}$
geometric	$v(x)^{\frac{1}{6}}\, s(x)^{\frac{1}{4}}$	$s(x)^{\frac{1}{2}}$	$\frac{v(x)}{s(x)}$
curvature 1	$v(x)^{\frac{1}{6}}\, s(x)^{\frac{1}{4}}$	$c(x)$	$\frac{v(x)}{s(x)}$
curvature 2	$v(x)^{\frac{1}{6}}\, s(x)^{\frac{1}{4}}$	$c(x)$	$c(x)$
$D_f = 1.8$	$v(x)^{-\frac{1}{9}}\, s(x)^{\frac{2}{3}}$	$s(x)^{\frac{1}{2}}$	$\frac{v(x)}{s(x)}$

Table 2: *Primary particle diameter calculated by linear regression*

	Diameter / nm		
height above burner	0.4 cm	1.4 cm	4.2 cm
Balthasar	24.2	38.4	39.4
geometric mean	24.3	38.4	39.5
$D_f = 1.8$	23.9	37.4	38.5
$D_f = 1.8$ sphere diameter for OH rate	25.4	39.7	40.8
curvature 1	23.7	37.5	38.6
curvature 2	22.9	36.4	37.5

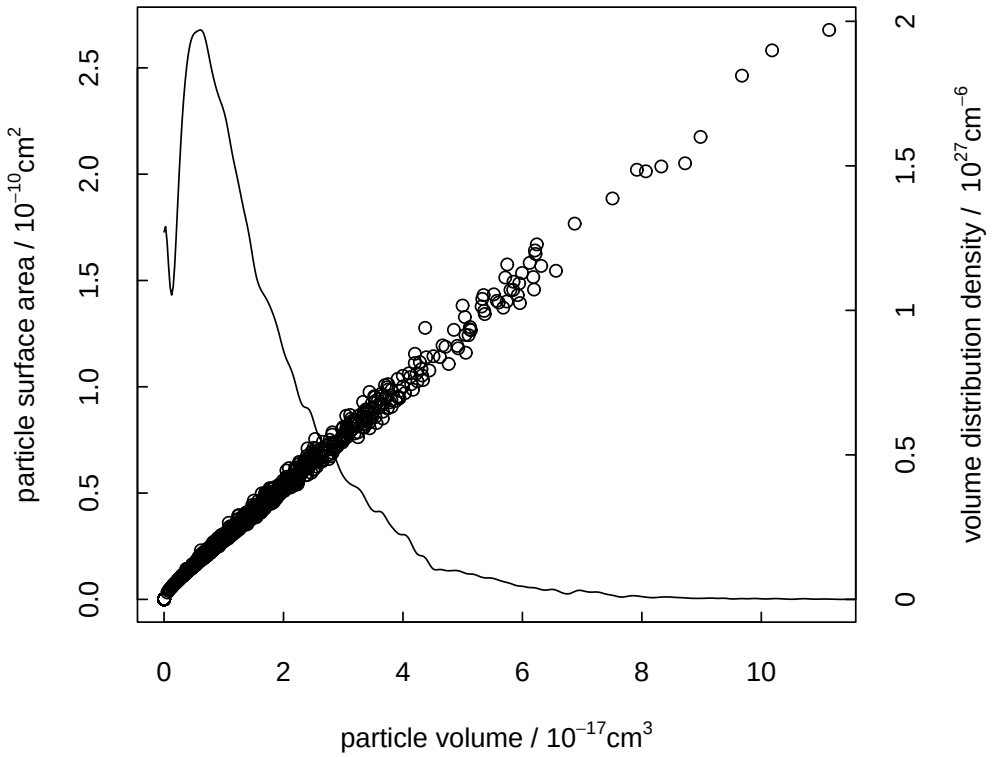

(a) 0.4 cm above burner

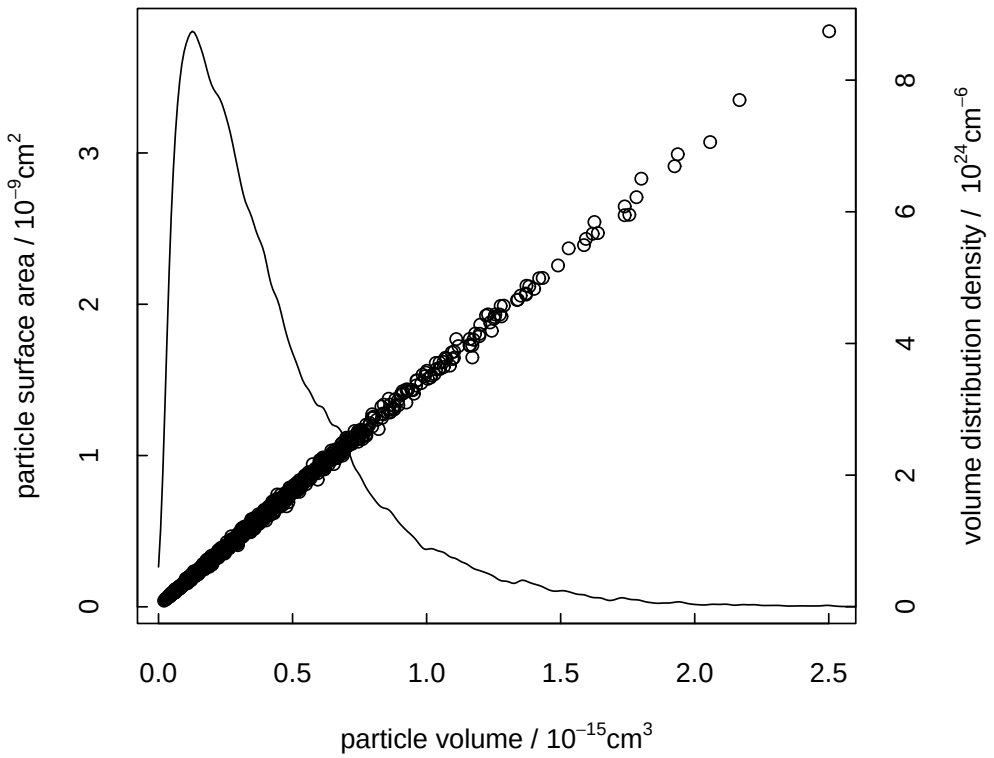

(b) 4.2 cm above burner

Figure 5: *Particle distributions*

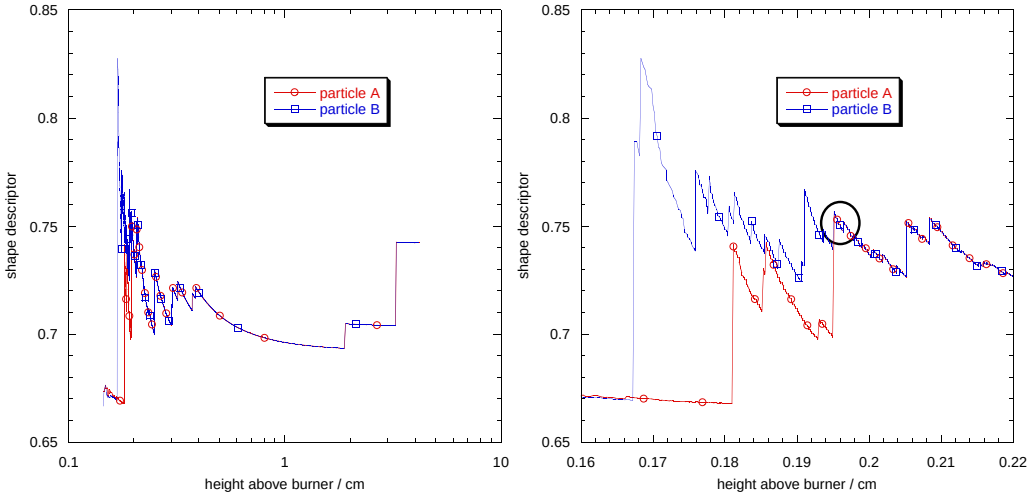

(a) Balthasar (b) shape detail for Balthasar model

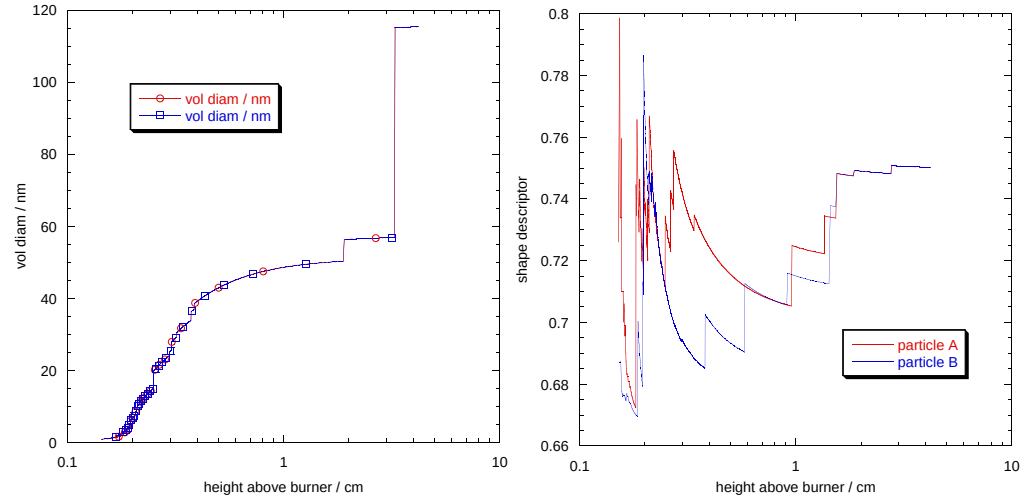

(c) size history (d) curvature 2

Figure 6: *Particles from flame JW10.673*

of the highly active early phase of the flame, even if the details within that zone are not resolved correctly.

That the fine structure of particles remains constant after the initial period of activity can also be seen from table 2, which gives the primary particle diameter calculated from the slope of the lines of least squares linear fit to the surface-volume distributions at three different heights above the burner. One can see that the slope, which is proportional to the diameter of table 2, changes noticeably over the first 1.5 cm of the flame but then hardly changes at all for the remainder of the flame. This is in accordance with figures 6(a) & 6(c) which show that surface processes which round out particles are only significant early in the flame and further from the burner all that happens is coagulation in which both the surface and the volume of the resulting particle is simply the sum of these two quantities for the incoming particles.

Figure 7 shows the shape descriptor of the first incepted particle and the mean for the first nineteen in a single simulation of JW10.673 using the Balthasar & Frenklach collision kernel (6) along with the population average calculated over twenty simulations. Unsurprisingly the first particles to form undergo more coagulation and hence develop a less spherical structure than particles which form later.

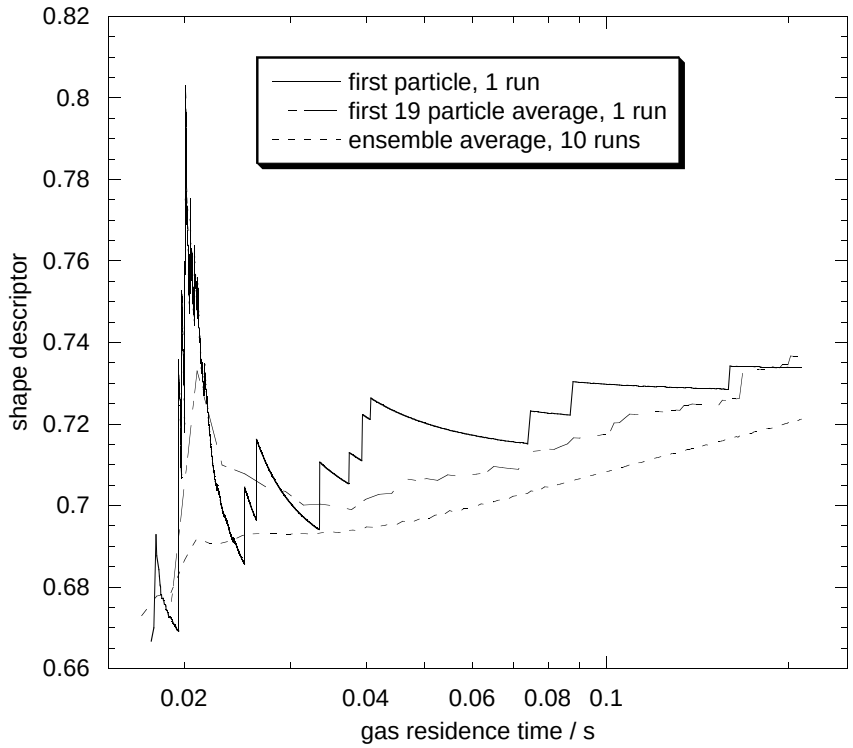

Figure 7: *Mean shape descriptors for JW10.673*

The difference between the shape descriptor averaged over the first nineteen particles and that averaged over the complete particle ensemble (between one and two thousand computational particles) explains some of the features of [3, figure 3]. In that paper Balthasar and Frenklach observe that for the flame JW10.673 the average shape descriptor of their

"collector particle" (one of the first particles to be incepted, see [18] for details) is much higher than the ensemble average calculated with their MoMIC approximation which is about 0.7 after 0.1 s and reaches about 0.72 after 0.2 s. These results tend to confirm the accuracy of their MoMIC approximation even though it assumes all particles have the same shape descriptor (which changes with time) and show that their Monte Carlo results are only applicable for the first few particles to be incepted. It should, however, be noted that the flame JW10.673 for which this comparison has been performed has a unimodal particle size distribution and that the MoMIC tends to perform well in such cases, but struggles with bimodal flames.

4.4 Additional Comparison

The preceding sections concentrate on comparisons between different variations of the bi-variate model presented in this paper. However, there is some recent work [20, 5], which uses a very intricate model for particle structure (which will be referred to as the 'detailed aggregate' model). The model in [20, 5] is a development of the work referred to in §3.1.1 and it enables some additional comparisons to be made to the work reported in this paper. In [20, 5] every aggregate soot particle is represented as a collection of intersection spheres so volume, surface area and collision diameter can all be calculated directly. Consequently for problems where coagulation leads to a rigid connection forming at the first point of contact between two particles the detailed aggregate model does not introduce any error. This is confirmed in [20] where the fractal dimension for aggregates undergoing ballistic collisions is checked and a value of 1.93 is found which is within the previously known range.

To test the ability of the bivariate code to model aggregate coagulation the flame A3 [41] considered in [20] was used but all processes except particle inception and coagulation were ignored. This gave a test of coagulation and results are shown in figure 8. Soot volume fraction (equivalent to the first moment of the mass distribution) is not considered because it is unaffected by coagulation. These results show that the assume fractal dimension of 1.8 is much more accurate than the other bivariate models, such as the geometric mean model which implicitly assumes a fractal dimension of 2.4 for the particles (see §3.1.4). Since the fractal dimension of the particles is known to be around 1.9 in this case such a result is not surprising.

Finally both codes were used to perform a full simulation of the flame A3; details of the physical model for inception, coagulation and surface reactions can be found in [29, 26, 1, 35]. Full flame simulations are important because flames are dominated by surface growth not coagulation [25]. Some results are given in figure 9 and show smaller differences between the models. The closer agreement may be explained by an increase in the fractal dimension of the soot particles, the detailed aggregate model simulations suggest a population average fractal dimension that slowly decreases from 3 to 2.75 as particles move through the flame.

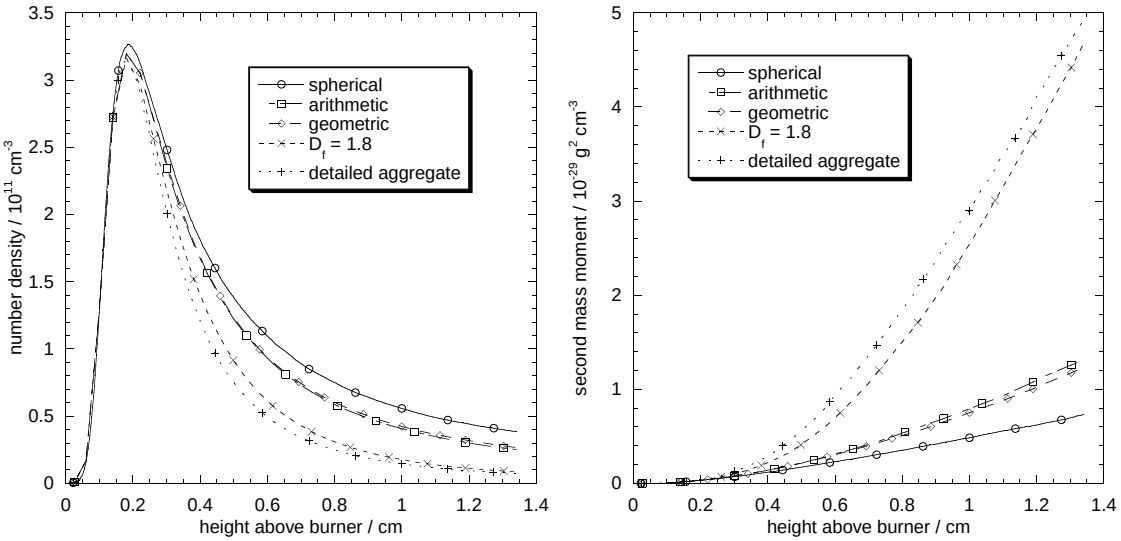

(a) Number density (b) Second moment

Figure 8: *Inception and coagulation only*

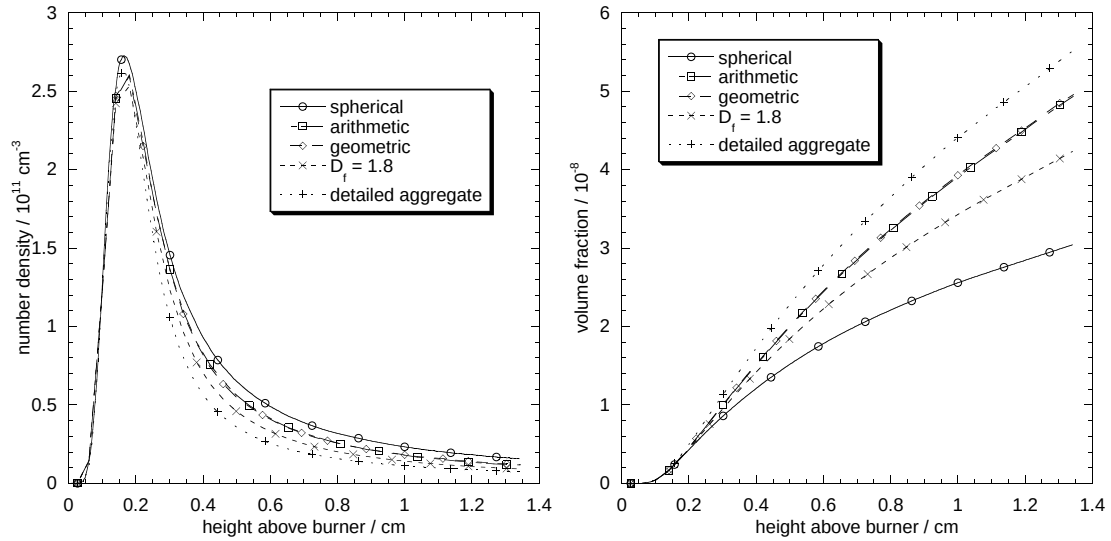

(a) Number density (b) Volume fraction

Figure 9: *Results for flame A3*

5 Conclusion

Principles for designing a simple, two variable model of aggregate soot formation have been introduced and tested for two laminar premixed flames. The predictions of this model, which reflects the non-spherical nature of soot particles, have been found to be quantitatively different from those of a single variable model which assumes particle sphericity. Using a Direct Simulation Algorithm the bivariate size and shape distribution functions have been calculated and individual particle histories analysed. These numerical investigations indicate that several collision diameter models derived in different ways lead to very similar bivariate distributions and, in particular, the model presented in [3] is consistent with some simple models suggested here. A simple, assumed fractal dimension model based on the work of Park and Rogak [22] leads to moderately different results because it leads to much higher rates of soot oxidation by OH radicals. Alternative models for surface curvature which specifies the geometric effect of surface reactions also lead to moderate changes in the bulk properties of the soot but not to qualitative differences in the soot formation process. Extremely detailed models for particle structure also seem to have very modest effects on results for simulations of real flames. However, the detailed aggregate simulations also suggest that the accuracy of bivariate models has a dependence on the fractal dimension of the soot particles.

Therefore, the simple particle shape models considered here offer a useful starting point for more detailed modelling of soot surface chemistry. The importance of including particle shape is clearly illustrated by the difference between the spherical particle model and all the extensions which conserve surface area during coagulation. More work on surface curvature, to understand how particles change shape as they undergo surface reactions and whether either the detailed aggregate model or a bivariate model can capture this, is needed. It seems likely that such work would be based on transmission electron micrographs of soot particles sampled from several positions in each of a range of flames. Nevertheless, all of the models which try to account for particle shape show similar deviations from the spherical particle model and so future work can, initially, make use of which ever models seem most convenient.

All the new models introduced in this paper are expressed as linear combinations of powers of the two components of the particle type/description. This makes it very simple to formulation moment equations for the soot population, something that will be demonstrated in a forthcoming paper.

6 Acknowledgements

Discussions with Prof. M Frenklach were very helpful in planning this work. The authors would like to thank Mr J Singh for his work in calculating chemical species profiles for the flames considered.

The support of the EPSRC under EP-C547241-1 and of Trinity College, Cambridge for RP is gratefully acknowledged. NM is grateful for support from the Haseldin fund of Clare College, Cambridge and the EPSRC under GR/R85662/01.

References

[1] J Appel, H Bockhorn, and M Frenklach. Kinetic modeling of soot formation with detailed chemistry and physics: Laminar premixed flames of C_2 hydrocarbons. Combust. Flame, 121:122–136, 2000.

[2] M Balthasar and M Kraft. A stochastic approach to solve the particle size distribution function of soot particles in laminar premixed flames. Combust. Flame, 133:289–298, 2003.

[3] Michael Balthasar and Michael Frenklach. Detailed kinetic modeling of soot aggregate formation in laminar premixed flames. Combust. Flame, 140:130–145, 2005.

[4] Michael Balthasar and Michael Frenklach. Monte-Carlo simulation of soot particle coagulation and aggregation: the effect of a realistic size distribution. Proc. Combust. Inst., (30):1467–1475, 2005.

[5] Michael Balthasar, Markus Kraft, and Michael Frenklach. Kinetic Monte-Carlo simulations of soot particle aggregation. American Chemical Society Preprint Papers, 50(1):135–136, 2005.

[6] A Braun, N Shah, F E Huggins, K E Kelly, A Sarofim, C Jacobsen, S Wirick, H Francis, J Ilavsky, G E Thomas, and G P Huffman. X-ray scattering and spectroscopy studies on diesel soot from oxygenated fuel under various engine load conditions. Carbon, 43:2588–2599, 2005.

[7] A Eibeck and W Wagner. Approximative solution of the coagulation-fragmentation equation by stochastic particle systems. Stochastic Anal. Appl., 18(6):921–948, 2000.

[8] M Frenklach. Method of moments with interpolative closure. Chem. Eng. Sci., 57:2229–2239, 2002.

[9] Compuational Modelling Group. Cambridge soot database. http://www.cheng.cam.ac.uk/research/groups/como/proj.database.html.

[10] Mark Z Jacobson and John H Seinfeld. Evolution of nanoparticle size and mixing state near the point of emission. Atmospheric Environment, 38:1839–1850, 2004.

[11] A Kazakov, H Wang, and M Frenklach. Detailed modeling of soot formation in laminar premixed ethylene flames at a pressure of 10 bar. Combust. Flame, 100:111–120, 1995.

[12] C H Kim, A M El-Leathy, F Xu, and G M Faeth. Soot surface growth and oxidation in laminar diffusion flames at pressures of 0.1-1.0 atm. Combust. Flame, 136:191–207, 2004.

[13] Margaritis Kostoglou and Athanasios G Konstandopoulos. Evolution of aggregate size and fractal dimension during Brownian coagulation. J. Aerosol Sci, 32:1399–1420, 2001.

[14] Ü Ö Küoylü, G M Faeth, T L Farias, and M G Carvalho. Fractal and projected structure properties of soot aggregates. Combust. Flame, 100:621–633, 1995.

[15] Ü Ö Küoylü, C S McEnally, D E Rosner, and L D Pfefferle. Simultaneous measurements of soot volume fraction and particle size / microstructure using a thermophoretic sampling technique. Combust. Flame, 109:488–500, 1996.

[16] Zhigang Li and Hai Wang. Drag force, diffusion coefficient, and electric mobility of small particles. II. Application. Phys. Rev. E, 68:061207, 2003.

[17] P Mitchell and M Frenklach. Monte Carlo simulation of soot aggregation with simultaneous surface growth - why primary particles appear spherical. In 27th Symposium (International) on Combustion, pages 1507–1514. Combustion Institute, 1998.

[18] P A Mitchell. Monte Carlo Simulation of Soot Aggregation with Simultaneous Surface Growth. PhD thesis, University of California, Berkeley, 2001.

[19] Pablo Mitchell and Michael Frenklach. Particle aggregation with simultaneous surface growth. Phys. Rev. E, 67:061407, 2003.

[20] N Morgan, M Kraft, M Balthasar, D Wong, M Frenklach, and P Mitchell. Numerical nimulations of soot aggregation in premixed laminar flames. In Proceedings of the Combustion Institute. Combustion Institute, 2006. in press.

[21] Berk Öktem, Michael P Tolocka, Bin Zhao, Hai Wang, and Murray V Johnston. Chemical species associated with the early stage of soot growth in a laminar premixed ethyleneoxygenargon flame. Combust. Flame, 142:364–373, 2005.

[22] S H Park and S N Rogak. A one-dimensional model for coagulation, sintering, and surface growth of aerosol agglomerates. Aerosol Sci. Tech., 37:947–960, 2003.

[23] S H Park and S N Rogak. A novel fixed-sectional model for the formation and growth of aerosol agglomerates. J. Aerosol Sci., 35:1385–1404, 2004.

[24] S H Park, S N Rogak, W K Bushe, J Z Wen, and M J Thomson. An aerosol model to predict size and structure of soot particles. Combust. Theory Model., 9(3):499–513, 2005.

[25] R I A Patterson, J Singh, M Balthasar, M Kraft, and J R Norris. The linear process deferment algorithm: A new technique for solving population balance equations. SIAM J. Sci. Comput., 145(1):303–320, 2006.

[26] Robert Patterson, Jasdeep Singh, Michael Balthasar, Markus Kraft, and Wolfgang Wagner. Extending stochastic soot simulation to higher pressures. Combust. Flame, 145(3):638–642, 2006.

[27] R Development Core Team. R: A language and environment for statistical computing. R Foundation for Statistical Computing, Vienna, Austria, 2005. ISBN 3-900051-07-0.

[28] Kenneth L Revzan, Nancy J Brown, and Michael Frenklach. http://www.me.berkeley.edu/soot/.

[29] J Singh, R Patterson, M Balthasar, M Kraft, and W Wagner. Modelling soot particle size distribution: Dynamics of pressure regimes. Technical Report 25, c4e Preprint-Series, Cambridge, 2004.

[30] C M Sorensen. Light scattering by fractal aggregates: A review. Aerosol Sci. Tech., 35:648–687, 2001.

[31] C M Sorensen, J Cai, and N Lu. Light-scattering measurements of monomer size, monomers per aggregate, and fractal dimension for soot aggregates in flames. Applied Optics, 31(30):6547–6557, 1992.

[32] C M Sorensen and G D Feke. Post flame soot. In D P Lund and E A Angell, editors, Proceedings of the International Conference on Fire Research and Engineering, pages 280–285, Boston, MA, 1995. Society of Fire Protection Engineers.

[33] Stavros Tsantilis and Sotiris E Pratsinis. Soft- and hard-agglomerate aerosols made at high temperatures. Langmuir, 20(14):5933–5939, 2004.

[34] W N Venables and B D Ripley. Modern Applied Statistics with S. Springer, 4th edition, 2002.

[35] H Wang and M Frenklach. A detailed kinetic modeling study of aromatics formation in laminar premixed acetylene and ethylene flames. Combust. Flame, 110:173–221, 1997.

[36] Hai Wang, Bin Shao, Barbara Wyslouzil, and Kiril Streletzky. Small-angle neutron scattering of soot formed in laminar premixed ethylene flames. Proc. Combust. Inst., 29:2749–2757, 2002.

[37] J Z Wen, M J Thomson, and M F Lightstone. Numerical study of carbonaceous nanoparticle formation behind shock waves. Combust. Theory Model., 2005. in press.

[38] John Z Wen, M J Thompson, S H Park, S N Rogak, and M F Lightstone. Study of soot growth in a plug flow reactor using a moving sectional model. Proc. Combust. Inst., 30:1477–1484, 2005.

[39] F Xu, K C Lin, and G M Faeth. Soot formation in laminar premixed methane/oxygen flames at atmospheric pressure. Combust. Flame, 115:195–209, 1998.

[40] F Xu, P B Sunderland, and G M Faeth. Soot formation in laminar premixed ethylene/air flames at atmospheric pressure. Combust. Flame, 108:471–493, 1997.

[41] Bin Zhao, Zhiwei Yang, Zhigang Li, Murray V Johnston, and Hai Wang. Particle size distribution function of incipient soot in laminar premixed ethylene flames: effect of flame temperature. In 30th Symposium (International) on Combustion. Combustion Institute, 2004.